Received: 26 April 2022 | Accepted: 28 April 2022

DOI: 10.1111/arcm.12785

ORIGINAL ARTICLE

Electrochemical methods to discriminate technology and provenance of Apulian red-figured pottery. I. VIMP and SECM

Antonio Doménech-Carbó[1] | **Michele Giannuzzi**[2] | **Annarosa Mangone**[2,3] | **Lorena Carla Giannossa**[2,3]

[1]Departament de Química Analítica, Universitat de València, Burjassot, València, Spain

[2]Dipartimento di Chimica, Università degli Studi di Bari 'Aldo Moro', Bari, Italy

[3]Centro Interdipartimentale Laboratorio di Ricerca per la Diagnostica dei Beni Culturali, Universitat de València, Bari, Italy

Correspondence
Antonio Doménech-Carbó, Departament de Química Analítica, Universitat de València, Dr. Moliner 50, 46100 Burjassot (València), Spain.
Email: antonio.domenech@uv.es

Funding information
Ministerio de Ciencia e Innovación, Agencia Estatal de Investigación, Grant/Award Number: PID2020-113022GB-I00

Abstract

Voltammetry of immobilized particles (VIMP) and scanning electrochemical microscopy techniques are combined to study nanosamples from 60 Apulian red-figured pottery objects from six Apulian archaeological sites (Altamura, Arpi, Conversano, Egnazia, Monte Sannace, Taranto) and three Attic samples from Pella. The VIMP signatures corresponding to the electrocatalytic effect of microparticulate deposits of the clay body and the black gloss on the oxygen evolution reaction and the oxygen reduction reaction are obtained. These signatures provide information on the reducing/oxidizing conditions of firing. The combination of the above voltammetric data permits us to distinguish between Apulian production and Attic importations as well as to discriminate the productions from different archaeological sites or even within different technologies in samples from the same site.

KEYWORDS

Apulian red-figured pottery, archaeometry, electrocatalysis, electrochemistry

INTRODUCTION

Apulian red-figured pottery has been widely studied because of its excellent drawing ability and remarkable quality (Beazley, 1963; Trendall, 1967; Trendall & Cambitoglou, 1978, 1982). This

pottery was produced within the 5th and 4th centuries BCE (typically between 450 and 300 BCE) and was based on painting on the vase a black glossy background, saving figures from the ceramic body. The production has been formally divided into three periods: Early (430–370 BCE), Middle (from 370 to 340–330 BCE) and Late Apulian (340–300 BCE) (Trendall, 1989).

This pottery is directly related to the preceding Attic production, characterized by the fine texture of the ceramic body and the direct painting of the black gloss on the ceramic body. During the 4th century, however, in the Apulian sites, a new technology appears (Eramo & Mangone, 2019; Giannossa et al., 2017, 2021; Mangone et al., 2008, 2013). A part of the Apulian production has the characteristics of the Attic production, but a second group is characterized by the coarse texture of the ceramic body and the application of a red engobe layer on the clay paste, before the black gloss painting. Accordingly, there is debate about the technical characteristics of the Apulian red-figured pottery, in particular whether local production mimicked Attic manufacturing procedures or developed new methodologies, whether generalized techniques or local variants were produced, including the conditions of firing (more or less reducing/oxidizing conditions, one- or two-step firings) (Eramo & Mangone, 2019; Giannossa et al., 2017, 2021; Ingo et al., 2000; Mangone et al., 2008, 2009, 2013; Maniatis et al., 1993; Mirti et al., 2004, 2006; Tang et al., 2001; Thorn & Glascock, 2010; Tite et al., 1982). The elucidation of these matters is made difficult by the absence of historical sources describing the technical aspects of the production, the coexistence of local with imported productions in archaeological sites, and the intrinsic difficulties of the chemical and mineralogical analyses of ceramic materials.

In this context, recent research has characterized peculiar features of Apulian red-figured pottery in the 4th century BCE, different from the Attic one based on electron microscopy, X-ray diffraction and atomic spectroscopy techniques (Eramo & Mangone, 2019; Giannossa et al., 2017, 2019, 2020, 2021). The purpose of the current work is to describe the application of a solid-state electrochemistry technique, the voltammetry of immobilized particles (VIMP) to the characterization of provenances and manufacturing techniques of Apulian red-figured pottery and, in particular, its relationship with Attic production. The VIMP is a technique developed by Scholz and Meyer (1998) and Scholz et al. (2014) based on the abrasive transference of a small amount of solid sample (of few nanograms) to the surface of an inert electrode (paraffin-impregnated graphite). The record of its voltammetric response in contact with a suitable electrolyte where the solid is sparingly soluble permits us to acquire compositional thermochemical and even structural data on the solid material (Doménech-Carbó et al., 2013; Scholz et al., 2014). Due to its inherent sensitivity and essentially non-destructive character, the VIMP has been extensively used in the fields of archaeometry, conservation and restoration (Doménech-Carbó, 2010; Doménech-Carbó & Doménech-Carbó, 2018; Doménech-Carbó et al., 2009), in particular being applied to the study of ceramic and glass materials (Di Turo et al., 2018; Doménech-Carbó et al., 2002, 2019; Fabrizzi et al., 2020; Ramaciotti et al., 2020; Sánchez-Ramos et al., 2002).

In the current report, we describe the application of VIMP methodology to a set of samples from some of the most important Apulian sites: Altamura (Bari), Arpi (Foggia), Conversano (Bari), Monte Sannace (Gioia del Colle, Bari), Egnatia (Fasano, Brindisi), and Taranto as well as three Attic samples from Pella. This study is aimed to elucidate the possibility of an electrochemical discrimination of sites and/or manufacturing techniques studying separately the voltammetric response of the clay body and black gloss layer.

This study is based on the systematic evaluation of electrocatalytic effects exerted by ceramic materials on the oxygen evolution reaction (OER) and oxygen reduction reaction (ORR) processes. These are particularly intense for a ubiquitous component of ceramic materials, haematite, which has recognized electrocatalytic ability towards such processes (Bouhjar et al., 2018; Peter, 2013; Shimizu, Sepunaru, & Compton, 2016; Shimizu, Tschulik & Compton, 2016; Wan et al., 2019; Zhu et al., 2013), but also by hercynite, an iron spinel characterizing black glosses

(Zhao et al., 2017). Previously (Doménech-Carbó et al., 2022), we studied these catalytic processes in haematites, iron earths and some Apulian ceramic pastes combining VIMP and scanning electrochemical microscopy (SECM). Here, we extend the number of samples and sites and apply this methodology not only to clay bodies but also to black glosses, the most remarkable feature of this type of ceramics. VIMP measurements were complemented with SECM where the application of the redox competition methodology (Henrotte et al., 2020) to SECM permits us to detect local electrocatalytic activity of surfaces at the nanoscopic scale, as previously applied in the study of pigments in paintings (Doménech-Carbó et al., 2015).

In this regard it is pertinent to mention that the voltammetric response of pottery samples in contact with aqueous electrolytes mainly involves the reduction of Fe(III) minerals (haematite, Fe_2O_3; goethite, FeO(OH)), of widely studied solid-state electrochemistry (Grygar, 1996, 1997; Shimizu, Tschulik, & Compton, 2016), and the oxidation of Fe(II) ones (fayalite, Fe_2SiO_4; chrysolite, $(Mg,Fe)_2SiO_4$; augite, $Ca_{0.61}Mg_{0.76}Fe_{0.49}(SiO_3)_2$). In the case of black glosses, these are composed of different stable or metastable Fe oxides with spinel structure such as maghemite, magnetite often accompanied by ilmenite and wüstite and mixed crystals of hercynite ($FeAl_2O_4$), embedded in vitreous or partly crystalline matrices (Giannossa et al., 2019; Ingo et al., 2000; Lühl et al., 2014; Tang et al., 2001). The proposed methodology provides information on the manufacturing techniques, including firing temperature and possible multiple firing protocols, to some extent a controversial matter (Fontannaz, 2005; Lühl et al., 2014; Robinson, 2014; Thorn, 2009; Walton et al., 2013).

EXPERIMENTAL

Samples

Apulian samples comprised 13 from Monte Sannace (MS1, M8, M9, M14, M25, M28, M29, M31, AM2, AM3, AM4, AM6, AM7), five from Altamura (A4, A5, A8, A9, A11), one from Conversano (Co1), 13 from Egnatia (Egn1, Egn4, Egn6, Egn13, Egn25, Egn29, Egn33, Egn35, Egn39, Egn4N, Egn24N, Egn1P, Egn5P), 13 from Arpi, 10 coming from the ONC28 tomb (I1-01, I2-01, I3-01, C1-01, C7-01, A1-01, F-01, Ar4, Ar5, C5), and three coming from the Niobidi's tomb (AN5, AN8, AN10) and 15 from Taranto (212411, 227007, 227093, 227130, 227141, 227161, 227183, 227185, 227186, 227197, 227204, 227229, 227236, 227237 and 52231B). Attic samples consisted of three fragments from Pella (Pella1 to Pella3). Unbroken and reassembled items, as well as fragments, have been analysed. A photographic image of some examples representative of the finds analysed is provided as Supporting Information (Figure S.1).

Instrumentation and methods

Voltammetry measurements were performed at 298 K in a three-electrode cell using a CH I660C potentiostatic device (Cambria Scientific, Llwynhendy, Llanelli, UK) using air-saturated aqueous 0.10 M HCl (Panreac reagents) as a supporting electrolyte. Commercial graphite bars (Alpino Maxim HB-type, 2 mm diameter) were used as working electrodes, completing the three-electrode arrangement with a platinum disc auxiliary electrode and an Ag/AgCl (3 M NaCl) reference electrode. Square wave voltammetry (SWV) was used as the detection mode.

VIMP analysis of the red ceramic body was carried out by scratching ~1 μg of solid material from the cross-section of the fragments with the help of a scalpel. The ceramic material was distributed forming a fine layer onto one plane face of an agate mortar and then aliquots of the same were abrasively transferred to the graphite electrode as in typical VIMP experiments (Scholz & Meyer, 1998; Scholz et al., 2014). Sampling in the black gloss was carried out by

pressing the graphite bar directly onto the surface of the black surface of the ceramic fragments. In both cases, the sample-modified electrode was then dipped into the electrochemical cell so that only the lower end of the electrode was in contact with the electrolyte solution, and the voltammograms were recorded. To avoid possible biased selection of samples, these were randomized prior to voltammetric experiments.

SECM experiments were performed with CH 920c equipment using a microdisc platinum electrode tip (CH 49, diameter 20 μm) and a Pt disc electrode (geometrical area 0.018 cm^2) covered with a fine bed of carbon paste (graphite powder plus paraffin oil). Ceramic samples (∼1 μg) were deposited onto the carbon paste layer. The bipotentiostat mode was used to apply potentials to the tip (E_T) and the electrode substrate (E_S). The rate of scanning of the tip over the substrate was 20 μm/s for all experiments, the distance between tip and substrate being of the order of the tip electrode radius. Air-saturated 0.10 M HCl aqueous solution was used as the electrolyte in order to use the reduction of dissolved oxygen as a redox probe (Doménech-Carbó et al., 2015).

RESULTS AND DISCUSSION

VIMP

Figure 1 shows the SWVs recorded for the black gloss of samples (a,b) 52231B and (c,d) AN5 in contact with air-saturated 0.10 M HCl aqueous solution in negative-going (a,c) and positive-going (b,d) potential scans. According to the predominance of non-electroactive silicate and aluminosilicate species in ceramic samples, this voltammetry is dominated by the background processes of

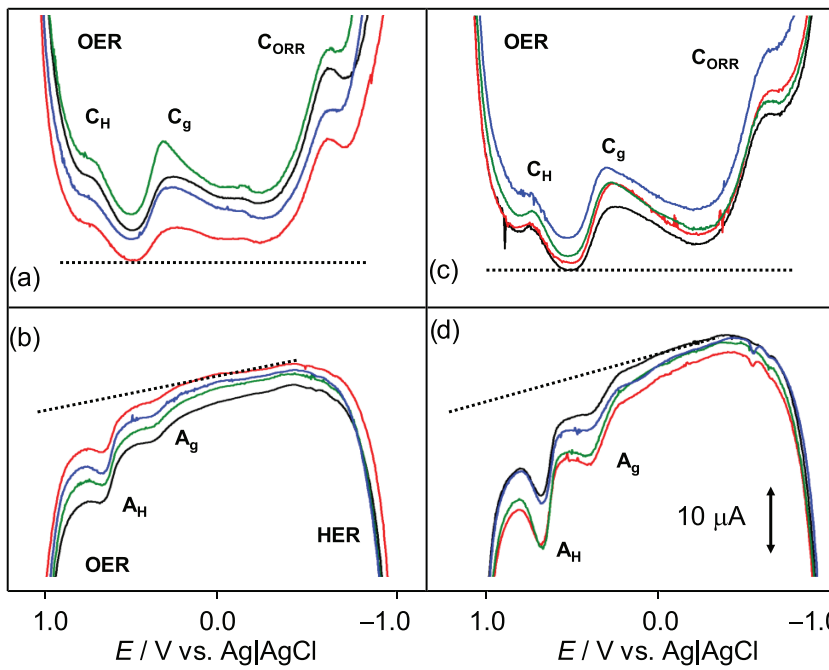

FIGURE 1 Square wave voltammetry of samples (a,b) 52231B and (c,d) AN5 transferred onto a graphite electrode in contact with air-saturated 0.10 M HCl aqueous solution. Potential scan initiated at: (a,c) 1.05 V in the negative direction, (b,d) −0.95 V in the positive direction. Potential step increment 4 mV; square wave amplitude 25 mV; frequency 10 Hz. The dotted lines mark the base lines used to measure peak currents denoted by double arrows

OER ~1.0 V versus Ag/AgCl and hydrogen evolution reaction (HER) ~−1.0 V, accompanied by the reduction of dissolved oxygen (ORR) at −0.65 V (C_{ORR}). In the potential region between 0.4 and −0.4 V weak cathodic and anodic signals appear. These can be attributed the reduction of Fe(III) compounds, mainly oxohydroxides, and the oxidation of Fe(II) ones. That which appears in both negative- and positive-going potential scan voltammograms at ~0.8 V can be associated (at least mainly) with the oxidation of haematite (C_H, A_H), as judged by the similarity of the voltammetric response to that of clay bodies and haematites. The oxidation process can be represented as follows (Doménech-Carbó et al., 2022):

$$Fe^{III}{}_2O_3 + 2xH_2O \rightarrow Fe^{IV}{}_xFe^{III}{}_{2-x}O_3(OH)_{2x} + 2xH^+ + 2xe^-. \quad (1)$$

As previously noted, both OER and ORR processes can be catalysed by some of the components of the sample, haematite in particular. This compound is a recognized catalyst and photocatalyst for the OER process (Bouhjar et al., 2018; Peter, 2013; Shimizu, Sepunaru, & Compton, 2016; Shimizu, Tschulik, & Compton, 2016; Wan et al., 2019; Zhu et al., 2013), a role conceivably played by other Fe(III) minerals. In turn, the A_H/C_H signals can be attributed to the oxidation of haematite to higher oxidation states of iron (IV, V and VI) (Cummings et al., 2011, 2012; Doménech-Carbó et al., 2021; Klahr & Hamman, 2014; Le Formal et al., 2010).

The catalytic ability of haematite on the electrochemical reduction of oxygen can be associated, according to Shimizu, Tschulik, and Compton (2016) with the increase in the rate of decomposition of hydrogen peroxide, an intermediate product in the ORR process. Consistently, prior data on haematite electrochemistry (Doménech-Carbó et al., 2022) revealed that the ORR signal is decreased on decreasing the crystallinity and degree of hydration of the mineral. Since the thermal treatment above ~500°C should dehydroxylate haematite, these features suggest that the intensity of the ORR signal can be representative of the firing temperature.

Additionally, Fe(II) minerals—spinels in particular (Zhao et al., 2017)—could also act as a catalyst for ORR. Although the ORR catalytic ability of haematite is mainly associated with the disproportionation of the intermediate H_2O_2 generated during O_2 reduction (Shimizu, Sepunaru, & Compton, 2016), a second reduction/regeneration mechanism can be proposed. This is supported by the recognition of the increased catalytic activity via activation by application of reductive potential inputs (Wan et al., 2019). This catalytic pathway involves the electrochemical generation of Fe(II) centres:

$$Fe_2O_3 + xH^+{}_{aq} + xe^- \rightarrow Fe^{III}{}_{2-x}Fe^{II}{}_xO_{3-x}(OH)_x, \quad (2)$$

which react with O_2, producing superoxide radical anion:

$$Fe^{III}{}_{2-x}Fe^{II}{}_xO_{3-x}(OH)_x + xH_2O + xO_2 \rightarrow Fe^{III}{}_2O_{3-x}(OH)_{2x} + xH^+{}_{aq} + xO_2{}^{\bullet -}. \quad (3)$$

The generated $O_2^{\bullet -}$ subsequently reacts to yield H_2O_2 and H_2O, whereas Fe(II) active sites are electrochemically regenerated:

$$Fe^{III}{}_2O_{3-x}(OH)_{2x} + xH^+{}_{aq} + xe^- \rightarrow Fe^{III}{}_{2-x}Fe^{II}{}_xO_{3-x}(OH)_x + xH_2O. \quad (4)$$

The catalysis of ORR by hercynite in principle results from the direct reaction with O_2:

$$Fe^{II}Al_2O_4 + xH_2O + xO_2 \rightarrow Fe^{III}{}_xFe^{II}{}_{1-x}Al_2O_4(OH)_x + xH^+{}_{aq} + xO_2{}^{\bullet -}, \quad (5)$$

accompanied by the electrochemical regeneration of the Fe(II) centres:

$$Fe^{III}{}_xFe^{II}{}_{1-x}Al_2O_4(OH)_x + xe^- \rightarrow Fe^{II}Al_2O_4 + xH_2O. \quad (6)$$

The electrochemical activation of haematite could involve the replacement of some O^{2-} ions by OH^- ones coupled to the Fe^{3+} to Fe^{2+} reduction (Ruan et al., 2001).

SECM

Figure 2 shows a colour graph and SECM topographic images of a microparticulate deposit of the clay body of sample 211412 forming a fine layer on a carbon paste substrate in contact with air-saturated 0.10 M HCl. SECM images were recorded by fixing the tip potential (E_T) at a value where the oxidation of dissolved oxygen occurs at −0.45 V, as previously determined voltammetrically. When no potential was applied to the substrate (Figure 2a,b), the exposed regions of the base electrode (marked by white arrows) yield a positive feedback response, whereas the regions covered by the clay body display negative feedback and a peaked topography. According to the redox competition methodology (Henrotte et al., 2020), when a potential activating haematite (−0.45 V) to act as ORR catalyst is applied to the substrate (E_S), the regions concentrating catalytically active centres, display enhanced tip currents (continuous black arrows). In contrast, the tip current in the regions poor in such catalytically active centres

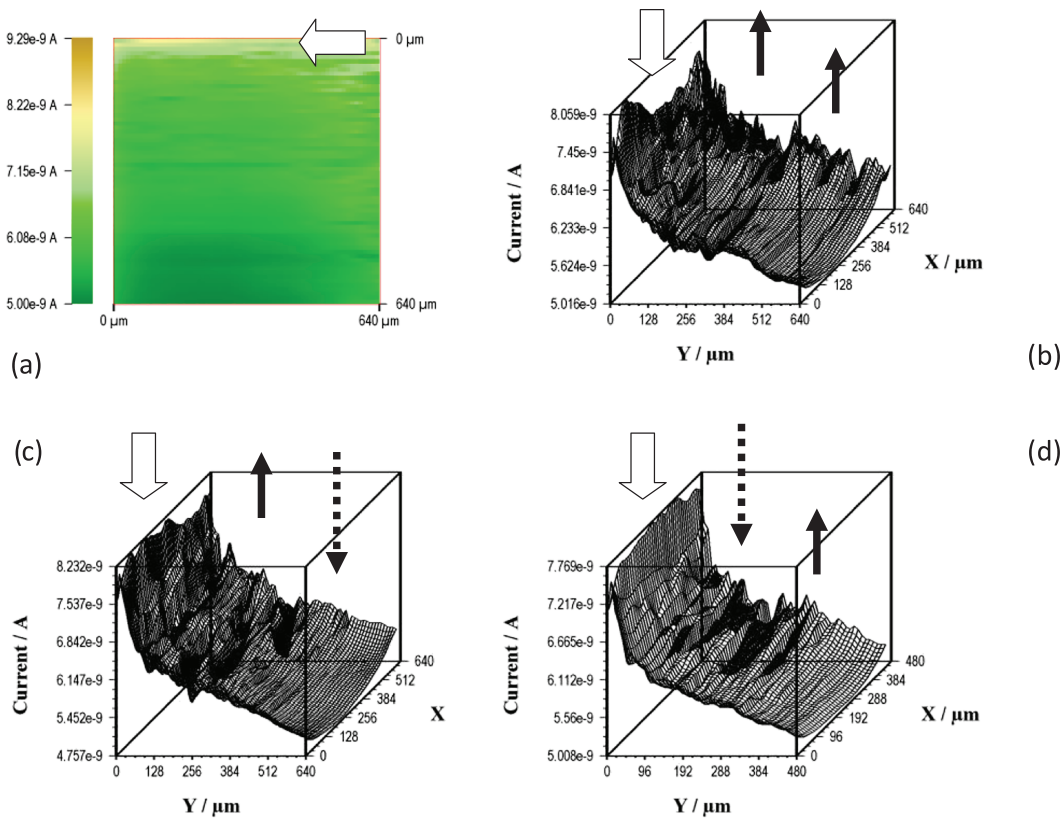

FIGURE 2 Colour (a) and (b–d) topographic scanning electrochemical microscopical images of Taranto sample 211412 on carbon paste substrate immersed in air-saturated 0.10 M HCl. (a,b) $E_T = -0.45$ V; $E_S = 0.00$ V; (c) $E_T = -0.45$ V; $E_S = -0.45$ V; (d) $E_T = -0.45$ V; $E_S = 1.00$ V

becomes depleted (dotted arrows) (Figure 2c). The inverse effect was observed when the substrate potential was moved to a value at which the A_H plus OER processes occur ($E_S = 1.0$ V). Now, the regions displaying increased and depleted tip currents are interchanged (Figure 2d). These features suggest that the ORR and OER processes are catalysed by different species, hercynite and haematite in the case of ORR, and hydroxylated haematite in the case of OER. This means that, to some extent, the ratio between the intensities of the C_{ORR} and C_H/A_H signals is representative of the crystallinity and degree of hydration of haematite and the proportion of Fe(II) and Fe(III) species in the ceramic materials.

In principle, the mineral components of pottery can also act as catalysts in the case of the signals at ~0.4 V (C_g and A_g) that can be attributed to the oxidation/reduction of oxygen functionalities (presumably of the quinone/catechol type) existing in the graphite surface (Noked et al., 2011).

For our purposes it is pertinent to emphasize two characteristics of our VIMP measurements: (i) the intensity of the voltammetric signals can in principle be taken as proportional of the net amount of electroactive species transferred onto the electrode surface, depending not only of the chemical composition but also on the crystallinity and particle shape and size; (ii) since the amount of sample effectively transferred onto the electrode cannot be accurately controlled, the absolute intensities of the signals cannot be reproduced in replicate experiments. The first of these characteristics implies that the observed voltammetric response depends not only on the mineralogical composition of the ceramic body but also on the compaction, grain size and degree of crystallinity of the sample, thus providing information on subtle differences between ceramic materials of slightly distinct origin. The second characteristic implies that signal intensity ratios or biparametric tendency curves have to be used to compare the VIMP behaviour of different samples.

Electrocatalysis and sample grouping

Considering the signals C_g,A_g, C_H/A_H and C_{ORR} we can apply a common scheme for the intensity of the signals based on theoretical models on the electrochemistry of redox-active solids (Lovrić & Scholz, 1997, 1999; Oldham, 1998; Schröder et al., 2000). As previously discussed, the signals C_H/A_H can mainly be attributed to the oxidation of Fe(III) species; haematite in particular (Le Formal et al., 2010, Cummings et al., 2011, 2012; Doménech-Carbó et al., 2021; Klahr & Hamman, 2014) overlapped with the catalysed OER. The intensity of the C_H peak will be representative of the net amount of such Fe(III) species (as well as their shape and size distribution and crystallinity). The signal C_{ORR} recorded in voltammograms such as in Figure 1 can be attributed to the reduction in dissolved oxygen catalysed either by haematite and other Fe(III) minerals and, in the case of black glosses, by hercynite and eventually other Fe(II) pristine species or electrochemically generated in the reduction of Fe(III) ones. As previously noted, the intensity of this peak will be to some extent representative of the net amount of such Fe(II) species. Finally, the signals C_g/A_g can mainly be attributed to the reduction/oxidation of oxygen functionalities existing (or electrochemically generated during the experiment) in the graphite surface. In principle, both Fe(III) (mainly) and Fe(II) species, among others, can act catalytically on this process.

Since the ceramic material forms a discontinuous microparticulate deposit on the graphite surface, the measured peak currents will reflect the contribution of the electrochemical process at the exposed graphite surface and the catalytic one promoted by the ceramic materials. This will be proportional to the net perimeter of the base electrode/ceramic particle/electrolyte junction. This can be taken as proportional to the area covered by the microparticulate deposit, S. Denoting by S_o the total area of the graphite electrode, the peak current (I_J) for the process J (J = H, OER, ORR, etc.) can be expressed as

$$I_J = g_J(S_o - S) + ph_J S, \tag{7}$$

where g_J represents the electrochemical coefficient of response of the J-process at the graphite surface, h_J is the corresponding coefficient for the catalytic process and p represents a geometrical coefficient relating the surface of the particles with their perimeter. This last coefficient will depend on the granulometry of the ceramic sample, whereas g_J, h_J are dependent on the process and the electrochemical parameters (electrolyte, potential scan rate, etc.). Since in replicate experiments the value of S will vary, one can characterize a given ceramic sample considering two electrochemical processes A, B. Then, eliminating S between the corresponding equations such as Equation (7), one obtains

$$\frac{I_A - g_A S_o}{ph_A - g_A} = \frac{I_B - g_B S_o}{ph_B - g_B}, \tag{8}$$

$$I_B = I_A\left(\frac{ph_B - g_B}{ph_A - g_A}\right) + S_o\left(g_B - g_A\frac{ph_B - g_B}{ph_A - g_A}\right). \tag{9}$$

This equation predicts that plot of I_B versus I_A should consist of a straight line whose slope and ordinate at the origin will be characteristic of each ceramic sample. Experimental data agree reasonably with this model as depicted in Supporting Information Figure S.2 for several clay body samples. One can see that, although there is relatively high data dispersion, the samples from each site fall within separate apparently linear tendency curves. Similar results (see below) were obtained in voltammograms of samples from the black gloss of the ceramic fragments. These differences reflect the different values of the ph_A and ph_B coefficients characterizing each ceramic production. The above treatment, however, is an oversimplification because the abrasive transference of the sample onto the graphite surface results in a variable effective surface due to the different surface scratching in each replicate measurement. This feature will be also influential on the relatively high data dispersion.

Voltammetric site analysis

The preceding analysis is entirely consistent with experimental data for the ceramic body and the black glaze layer. For instance, the plot of $I(C_{ORR})$ versus $I(C_H)$ recorded in SWVs in conditions such as in Figure 1 for Taranto samples clearly separates the data points of the ceramic body and the black glaze. As can be seen in Figure 3a, the $I(C_{ORR})$ values for the black glaze are always clearly larger than those for the clay body, in agreement with the expected larger proportion of Fe(II) species over Fe(III) ones in the black gloss relative to the clay body. This behaviour was observed from samples from Monte Sannace, Conversano and Pella. The difference between the clay body and the black gloss is low in the case of Altamura and Arpi (Figure 3b) (see Supporting Information, Figure S.3), whereas in the case of Egnatia samples there is the possibility of discriminating two different subsets (see below).

In principle, the differences in the recorded electrochemical responses can be attributed to differences in the manufacturing process, from the choice of raw materials to the refining, making and firing of the vase. In fact, clear differences can be seen even under the optical microscope with regard to the granulometry and presence of an engobe layer (see Supporting Information Figure S.4).

In spite of relatively high data dispersion, voltammetric data allow discriminatation of site-characteristic patterns. This can be seen in Figure 4, where plots of $I(C_{ORR})$ versus $I(C_H)$ corresponding to the black gloss of pottery samples in this study are depicted. As shown in

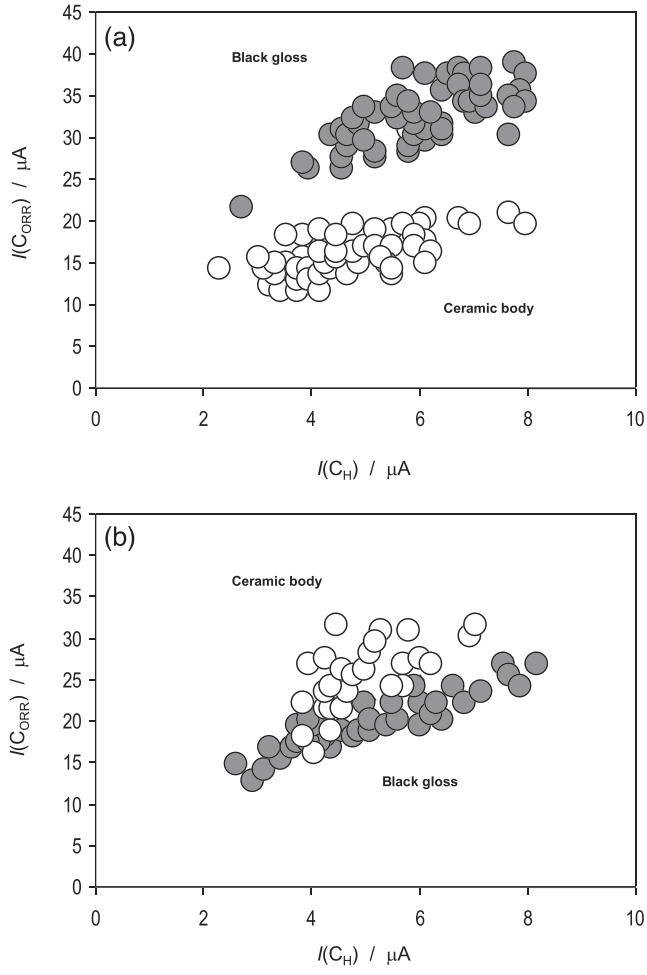

FIGURE 3 Plots of $I(C_{ORR})$ versus $I(C_H)$ recorded in SWVs in conditions such as in Figure 1 for Apulian red-figured pottery samples from: a) Taranto and b) Arpi, superimposing the data points for the black gloss (solid circles) and the ceramic body (circles)

Figure 4a, the data points of Taranto are clearly separated from those of Arpi. These representations permit discrimination of different sub-series within the same site. Thus the data points for samples from the ONC28 tomb in Arpi are separated from those of the Niobidi's tomb at the same archaeological site. Figure 4b compares the voltammetric data for Monte Sannace, Altamura and Pella. The samples from Monte Sannace are clearly separated from the Altamura and Pella samples. The data points for these last samples occupy the same region of the graph, in turn coincident with that occupied by the samples from the Niobidi's tomb in Arpi.

A second case where this discrimination can be clearly derived from electrocatalytic data is that of Egnatia samples. As can be seen in Supporting Information Figure S.5, a subset of the samples from this site, constituted by specimens Egn4N, Egn24N, Egn33, Egn1P and Egn5P, can be fitted to the Pella's pattern for both clay body (a) and black gloss (b) data representations. According to VIMP data, several samples, in particular including the Arpi AN5, AN8 and AN10 can be attributed to local production in 'Attic mode'. It is interesting to underline that Egn4N, Egn24N, Egn33, Egn1P and Egn5P are the only analysed finds from Egnatia made with the traditional technology (absence of engobe) (Mangone et al., 2013) and that AN5, AN8 and AN10 come from one of the richest funeral complexes in Daunia: the Niobidi's tomb (De Julius, 1992).

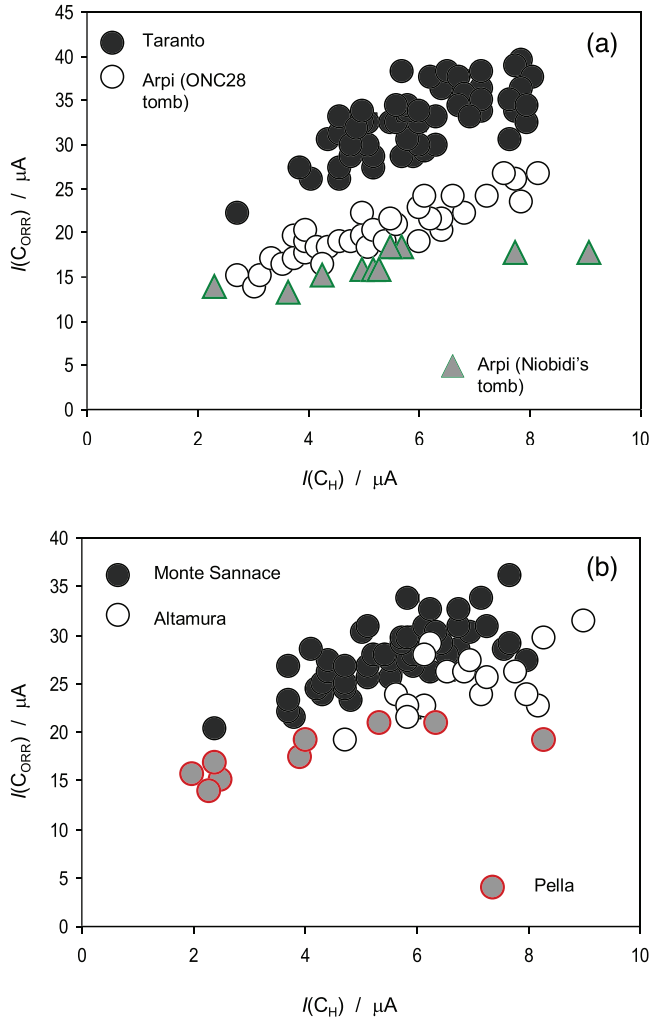

FIGURE 4 Plots of $I(C_{ORR})$ vs. $I(C_H)$ recorded by square wave voltammetry under conditions such as in Figure 1 for the black gloss of pottery samples from: (a) Taranto and Arpi; (b) Monte Sannace, Altamura and Pella

A clear discrimination between these and those fabricated in 'Apulian mode' can also be derived from the $I(C_{ORR})$ versus $I(C_g)$ representation presented in Figure 5, where both production modes become clearly separated. Interestingly, the two sets of samples can be fitted to different straight lines, in agreement with the previous theoretical approach.

Archaeometric implications

VIMP data—which are conditioned by the influence of mineralogical composition and granulometry on catalytic effects on OER and ORR processes—reflect, mainly, the proportion of catalytic species associated with haematite, hercynite and other iron minerals. Although other species in the sample may exert catalytic effects on these electrochemical processes, one can in principle assume that the ratio between the C_{ORR} and C_H signals, $I(C_{ORR})/I(C_H)$, is to some extent representative of the firing temperature and the apparent Fe(II)/Fe(III) ratio in the sample. This ratio is dependent on the composition of the raw materials, the firing temperature and

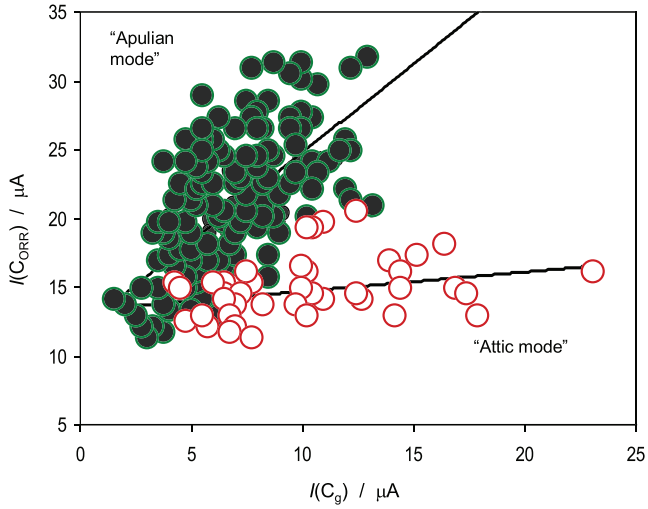

FIGURE 5 Plots of $I(C_{ORR})$ versus $I(C_g)$ recorded by square wave voltammetry under conditions such as in Figure 1 for Apulian red-figured pottery samples (clay body) in this study, separating the samples fabricated in Apulian and Attic modes. Continuous lines represent the fit of each subset of data to linear functions

the reducing/oxidizing conditions in the firing process. In this regard it is pertinent to note that haematite (and aluminous haematite (Ruan et al., 2001), which can appear as raw material or resulting from the dehydroxylation of goethite and other iron minerals, may differ in crystallinity depending on temperature. Although this is a matter for debate, it was suggested that some OH^- ions can substitute O^{2-} ones into the haematite lattice with concomitant replacement of Fe^{3+} ions by Fe^{2+} ones. Similarly, the reducing activation of haematite results in electrocatalytic activity on ORR (Wan et al., 2019).

Under this view, one can separate the samples from Taranto, Conversano and Monte Sannace as those showing higher $I(C_{ORR})/I(C_H)$ ratios in the black gloss relative to samples from Altamura, Arpi and Egnatia. On independently comparing electrochemical data for the clay body, the $I(C_{ORR})/I(C_H)$ ratio increases from Taranto and Monte Sannace to Altamura, Arpi, Conversano and Egnatia.

Actually, firing conditions are still under debate (Lühl et al., 2014; Robinson, 2014; Walton et al., 2013). In the early studies, it was hypothesized that all coverings were applied on the unfired vase and underwent a single firing process (Noble, 1960). However, considering the results of more recent archaeometric analyses on archaeological black gloss, Walton et al. (2013) questioned the hypothesis of a single firing, at least when black gloss and red overpainting with a very similar composition were present on the same vase. In this context, the existence of significantly different apparent $I(C_{ORR})/I(C_{OER})$ ratios in the black gloss and the ceramic body (see Figure 3) could be indicative of the application of successive firing steps during the fabrication of the vases.

To summarize, electrochemical data provide information on the apparent Fe(II)/Fe(III) ratio (and, ultimately, on the reducing/oxidizing conditions of firing) and the hardness, porosity, shape and size distribution of the ceramic material, here termed for brevity its 'granulometry'. The above considerations suggest that: (a) the studied pottery prepared in the 'Apulian mode'differed from the samples prepared in 'Attic mode' in both the 'granulometry' and/or firing conditions; (b) apparently, samples from Altamura, Arpi and Egnatia prepared the black gloss similarly to the Attic mode, whereas the production of Conversano, Monte Sannace and Taranto differed using more reducing conditions; (c) the clay body of Monte Sannace and Taranto presented properties similar to Attic samples in regard to the apparent Fe(II)/Fe(III) ratio, while all other samples, in particular those from Altamura, showed higher values of this parameter.

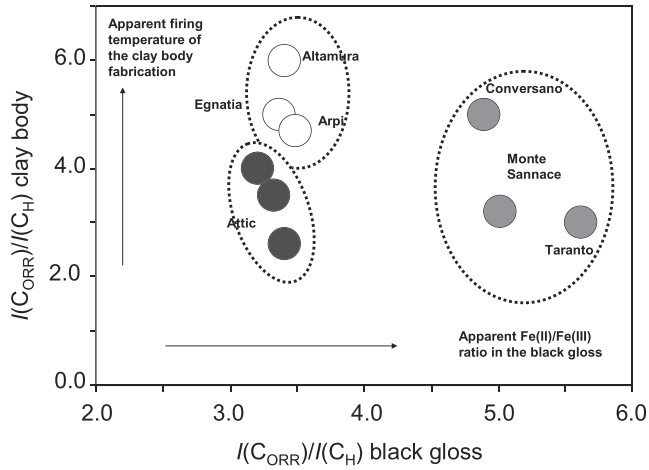

FIGURE 6 Two-dimensional diagram grouping the different sets of samples according to averaged $I(C_{ORR})/I(C_H)$ data for the black gloss and the clay body in this study

The foregoing set of considerations can be summarized using the two-dimensional diagram depicted in Figure 6, where the $I(C_{ORR})/I(C_H)$ ratios determined in VIMP experiments for the black gloss and clay body are plotted. Clearly, the electrochemical data draw a picture where the production of each site was distinctive, although reproducing more or less accurately some of the characteristics of the Attic pottery.

All results prove the existence of a polycentric production in Apulia during the Late period, at least regarding the manufacturing of ceramic bodies. For black glosses, on the other hand, the results obtained do not allow us to exclude the hypothesis of export of dried Attic black glaze to Greek colonies, as advanced by some scholars (Noble, 1960), at least for the samples of Arpi, Altamura and the samples 24N, 33N, 1P, 5P and 6P of Egnatia.

All this information is essential to map the production sites of finds and their transfer, and to trace the commercial routes. A geographical scheme showing the possible technological connections of the studied Apulian sites, here grouped as showing more or less close similarity to the Attic production mode, is provided as Supporting Information Figure S.6. It is in general believed that the red-figured pottery expanded from Taranto (Fontannaz, 2005; Robinson, 2014; Thorn, 2009), and current data suggest a complex scenario for this process of technology propagation in which the production in Altamura, Arpi and Egnatia was apparently closer to the Attic mode. Moreover, differences in the production technologies employed at the various sites can be retrieved by means of these results. The implementation of electrochemical techniques within the context of research on Apulian pottery enhances the scope of available techniques as a complementary analytical tool able to be used with samples at the microgram–nanogram level. They can help to understand the outstanding skill levels of Apulian potters in the 4th century BCE.

CONCLUSIONS

A series of 60 fragments of Apulian red-figured pottery coming from the archaeological sites of Altamura, Arpi, Conversano, Egnatia, Monte Sannace and Taranto and three fragments from the Greek site of Pella have been studied by means of VIMP and SECM techniques. Nanosamples from either the clay body or the black gloss of ceramic fragments attached to graphite electrodes in contact with air-saturated 0.10 M HCl display well-defined voltammetric responses. The catalytic enhancement of OER and ORR signals provide specific voltammetric

signatures that can be combined to obtain sample-characteristic and site-characteristic tendency curves that can be interpreted on the basis of a simple model. These can be considered as roughly representative of the Fe(II)/Fe(III) ratio in the samples, in turn informing on the more or less reducing/oxidizing firing conditions used during their manufacture.

Electrochemical data permit discrimination, using solely amounts of sample at the microgram level: (a) between the local Apulian production and the Attic one, identifying Attic importations recovered in the Apulian sites; (b) of the ceramic production manufactured in the Apulian sites; (c) of different types of production in each site. Additionally, electrochemical data provide information on the firing conditions of fabrication and on the granulometry of the clay body. Future research will improve knowledge of the electrochemical processes and their implications with regard to the elucidation of the ceramic manufacturing techniques, the discrimination of local varieties and even dating.

ACKNOWLEDGEMENTS

The work was carried out within the framework of project PID2020-113022GB-I00, which was financially support by *Ministerio de Ciencia e Innovación* and *Agencia Estatal de Investigación* (AEI) of the Spanish government.

PEER REVIEW

The peer review history for this article is available at https://publons.com/publon/10.1111/arcm.12785.

DATA AVAILABILITY STATEMENT

The data that support the findings in this study are included in the Supplementary Information.

ORCID

Antonio Doménech-Carbó https://orcid.org/0000-0002-5284-2811
Annarosa Mangone https://orcid.org/0000-0002-4757-1228

REFERENCES

Beazley, J. D. (1963). *Attic red-figure vase-painters* (2nd ed.). Oxford University Press.

Bouhjar, F., Bessaïs, B., & Marí, B. (2018). Ultrathin-layer α-Fe_2O_3 deposited under hematite for solar water splitting. *Journal of Solid State Electrochemistry*, *22*, 2347–2356.

Cummings, C. Y., Marken, F., Peter, L. M., Tahir, A. A. J., & Wijayantha, K. G. U. (2012). Kinetics and mechanism of light-driven oxygen evolution at thin film α-Fe_2O_3 electrodes. *Chemical Communications*, *48*, 2027–2029.

Cummings, C. Y., Marken, F., Peter, L. M., Upul Wijayantha, K. G., & Tahir, A. A. J. (2011). New Insights into Water Splitting at Mesoporous α-Fe_2O_3 Films: A Study by Modulated Transmittance and Impedance Spectroscopies. *Journal of the American Chemical Soiety*, *134*, 1228–1234.

De Julius, E. (1992). *La tomba del vaso dei Niobidi de Arpi*. Edipublia.

Di Turo, F., Montoya, N., Piquero-Cilla, J., De Vito, C., Coletti, F., De Luca, I., & Doménech-Carbó, A. (2018). Electrochemical discrimination of manufacturing types of pottery from *Magna Mater* Temple and Fora of *Nerva* and *Caesar* (Rome, Italy). *Applied Clay Science*, *162*, 305–310.

Doménech-Carbó, A. (2010). Voltammetric methods applied to identification, speciation, and quantification of analytes from works of art: an overview. *Journal of Solid State Electrochemistry*, *14*, 363–379.

Doménech-Carbó, A., & Doménech-Carbó, M. T. (2018). Electroanalytical techniques in archaeological and art conservation. *Pure and Applied Chemistry*, *90*, 447–462.

Doménech-Carbó, A., Doménech-Carbó, M. T., & Costa, V. (2009). In F. Scholz (Ed.), *Electrochemical Methods in Archaeometry, Conservation and Restoration*. Monographs in Electrochemistry series. Springer.

Doménech-Carbó, A., Doménech-Carbó, M. T., Silva, M., Valle-Algarra, F. M., Gimeno-Adelantado, J. V., Bosch-Reig, F., & Mateo-Castro, R. (2015). Screening and mapping pigments in paintings using scanning electrochemical microscopy (SECM). *Analyst*, *140*, 1065–1075.

Doménech-Carbó, A., Giannuzzi, M., Mangone, A., Giannossa, L. C., Di Turo, F., Cofini, E., & Doménech-Carbó, M. T. (2022). Hematite, an electrocatalytic marker for the study of archaeological clay bodies. A VIMP plus SECM study. *ChemElectroChem*, *9*, 59–68.

Doménech-Carbó, A., Labuda, J., & Scholz, F. (2013). Electroanalytical chemistry for the analysis of solids: characterization and classification (IUPAC Technical Report). *Pure and Applied Chemistry*, *85*, 609–631.

Doménech-Carbó, A., La-Torre Riveros, L., Huanasponcco, W., Quispe, D., Doménech-Carbó, M. T., Cabrera, C. R., Gutiérrez, M. C., & Carmona, K. (2019). A. Solid-state electrochemical analysis of Inka pottery from Qotakalli archaeological site in the Cusco (Perú) area. *Journal of Solid State Electrochemistry*, *23*, 1541–1552.

Doménech-Carbó, A., Sánchez-Ramos, S., Doménech-Carbó, M. T., Gimeno-Adelantado, J. V., Bosch-Reig, F., Yusá-Marco, D. J., & Saurí-Peris, M. C. (2002). Electrochemical determination of the Fe (III)/Fe (II) ratio in archaeological ceramic materials using carbon paste and composite electrodes. *Electroanalysis*, *14*, 685–696.

Eramo, G., & Mangone, A. (2019). Archaeometry of ceramic materials. *Physical Science Reviews*, *4*, 331–355.

Fabrizzi, L., Nigro, L., Cappella, F., Spagnoli, F., Guirguis, M., Niveau de Villedry, A. M., Doménech-Carbó, M. T., De Vito, C., & Doménech-Carbó, A. (2020). Discrimination and provenances of Phoenician Red Slip Ware using both the solid state electrochemistry and petrographic analyses. *Electroanalysis*, *32*, 258–270.

Fontannaz, D. (2005). La céramique proto-apulienne de Tarente: problèmes et perspectives dune recontextualisation. In M. Denoyelle, E. Lippolis, M. Mazzei, & C. Pouzadoux (Eds.), 21*La céramique apulienne Bilan et perspectives, Actes de la table ronde organisée par lEcole française de Rome en collaboration avec la Soprintendenza per i Beni archeologici della Puglia et le Centre Jean Bérard de Naples, 30 novembre-2 décembre 2000* (pp. 125–142). Collection du Centre Jean Bérard.

Giannossa, L. C., Forleo, T., & Mangone, A. (2021). The distinctive role of metal elements in archaeometry. The case of Apulian red figure pottery. *Applied Sciences*, *11*, 3073.

Giannossa, L. C., Mininni, R. M., Laviano, R., Mastrorocco, F., Caggiani, M. C., & Mangone, A. (2017). An archaeometric approach to gain knowledge on technology and provenance of Apulian red-figured pottery from Taranto. *Archaeological and Anthropological Sciences*, *9*, 1125–1135.

Giannossa, L. C., Muntoni, I. M., Laviano, R., & Mangone, A. (2019). Contribution of mineralogical and analytical techniques to investigate provenance and technologies of Hellenistic pottery from Arpi (Southern Italy). *Journal of Archaeological Science: Reports*, *24*, 729–737.

Giannossa, L. C., Muntoni, I. M., Laviano, R., & Mangone, A. (2020). Building a step by step result in archaeometry. Raw materials, provenance and production technology of Apulian Red Figure pottery. *Journal of Cultural Heritage*, *43*, 242–248.

Grygar, T. (1996). The electrochemical dissolution of iron (III) and chromium (III) oxides and ferrites under conditions of abrasive stripping voltammetry. *Journal of Electroanalytical Chemistry*, *405*, 117–125.

Grygar, T. (1997). Dissolution of pure and substituted goethites controlled by the surface reaction under conditions of abrasive stripping voltammetry. *Journal of Solid State Electrochemistry*, *1*, 77–82.

Henrotte, O., Boudet, A., Limani, N., Bergonzo, P., Zribi, B., Scorsone, E., Jousselme, B., & Cornut, R. (2020). Steady-State Electrocatalytic Activity Evaluation with the Redox Competition Mode of Scanning Electrochemical Microscopy: A Gold Probe and a Boron-Doped Diamond Substrate. *ChemElectroChem*, *7*, 4633–4640.

Ingo, G. M., Bultrini, G., de Caro, T., & Del Vais, C. (2000). Microchemical study of the black gloss on red and black-figured Attic vases. *Surface and Interface Analysis*, *30*, 101–105.

Klahr, B., & Hamann, T. (2014). Water Oxidation on Hematite Photoelectrodes: Insight into the Nature of Surface States through In Situ Spectroelectrochemistry. *Journal of Physical Chemistry C*, *118*, 10393–10399.

Le Formal, F., Grätzel, M., & Sivula, K. (2010). Controlling photoactivity in ultrathin hematite films for solar water-splitting. *Advanced Functional Materials*, *20*, 1099–1107.

Lovrić, M., & Scholz, F. (1997). A model for the propagation of a redox reaction through microcrystals. *Journal of Solid State Electrochemistry*, *1*, 108–113.

Lovrić, M., & Scholz, F. (1999). A model for the coupled transport of ions and electrons in redox conductive microcrystals. *Journal of Solid State Electrochemistry*, *3*, 172–175.

Lühl, L., Hesse, B., Mantouvalou, I., Wilke, M., Mahlkow, S., Aloupi-Siotis, E., & Kanngiesser, B. (2014). Confocal XANES and the Attic Black Glaze: The Three-Stage Firing Process through Modern Reproduction. *Analytical Chemistry*, *86*, 6924–6930.

Mangone, A., Caggiani, M. C., Giannossa, L. C., Eramo, G., Redavid, R., & Laviano, R. (2013). Diversified production of red figured pottery in Apulia (Southern Italy) in the late period. *Journal of Cultural Heritage*, *14*, 82–88.

Mangone, A., Giannossa, L. C., Ciancio, A., Laviano, R., & Traini, A. (2008). Technological features of Apulian red figured pottery. *Journal of Archaeological Science*, *35*, 1533–1541.

Mangone, A., Giannossa, L. C., Colafemmina, G., Laviano, R., & Traini, A. (2009). Use of various spectroscopy techniques to investigate raw materials and define processes in the overpainting of Apulian red figured pottery (4th century BC) from southern Italy. *Microchemical Journal*, *92*, 97–102.

Maniatis, Y., Aloupi, E., & Stalios, A. D. (1993). New evidence for the nature of the Attic black gloss. *Archaeometry*, *35*, 23–34.

Mirti, P., Gulmini, M., Perardi, A., Davit, P., & Elia, D. (2004). Technology of production of red figure pottery from Attic and southern Italian workshop. *Anaytical and Bioanaytical Chemistry*, *380*, 712–718.

Mirti, P., Perardi, A., & Gulmini, M. (2006). A scientific investigation of the provenance and technology of a black-figure amphora attributed to the Priam group. *Archaeometry*, *48*, 31–43.

Noble, J. V. (1960). The technique of Attic vase-painting. *American Journal of Archaeology*, *64*, 307–313.
Noked, M., Soffer, A., & Aurbach, D. (2011). The electrochemistry of activated carbonaceous materials: past, present, and future. *Journal of Solid State Electrochemistry*, *15*, 1563–1578.
Oldham, K. B. (1998). Voltammetry at a three-phase junction. *Journal of Solid State Electrochemistry*, *2*, 367–377.
Peter, L. M. (2013). Energetics and kinetics of light-driven oxygen evolution at semiconductor electrodes: the example of hematite. *Journal of Solid State Electrochemistry*, *17*, 315–326.
Ramaciotti, M., Gallello, G., Navarro, D., Doménech-Carbó, A., Roldán, C., Hernández, E., Garrigues, S., & Pastor, A. (2020). A unique multi-analytical approach based on spectroscopic and electrochemical techniques to study composite Roman amphorae collection. *Applied Clay Science*, *198*, 105857.
Robinson, E. (2014). The early phases of Apulian red figure. In The regional production of red-figure pottery: Greece. In S. Schierup & V. Sabetai (Eds.), *Magna Graecia and Etruria* (pp. 217–233). Aarhus University Press.
Ruan, H. D., Frost, R. L., & Kloprogge, J. T. (2001). The behavior of hydroxyl units of synthetic goethite and its dehydroxylated product hematite. *Spectrochimica Acta A*, *57*, 2575–2586.
Sánchez-Ramos, S., Bosch-Reig, F., Gimeno-Adelantado, J. V., Yusá-Marco, D. J., & Doménech-Carbó, A. (2002). Application of XRF, XRD, thermal analysis and voltammetric techniques to the study of ancient ceramics. *Analytical and Bioanalytical Chemistry*, *373*, 893–900.
Scholz, F., & Meyer, B. (1998). Voltammetry of solid microparticles immobilized on electrode surfaces. In A. J. Bard & I. Rubinstein (Eds.), *Electroanalytical Chemistry, A Series of Advances* (Vol. 20) (pp. 1–86). Marcel Dekker.
Scholz, F., Schröder, U., Gulabowski, R., & Doménech-Carbó, A. (2014). *Electrochemistry of Immobilized Particles and Droplets* (2nd ed.). Springer.
Schröder, U., Oldham, K. B., Myland, J. C., Mahon, P. J., & Scholz, F. (2000). Modelling of solid state voltammetry of immobilized microcrystals assuming an initiation of the electrochemical reaction at a three-phase junction. *Journal of Solid State Electrochemistry*, *4*, 314–324.
Shimizu, K., Sepunaru, L., & Compton, R. G. (2016). Innovative catalyst design for the oxygen reduction reaction for fuel cells. *Chemical Science*, *7*, 3364–3369.
Shimizu, K., Tschulik, K., & Compton, R. G. (2016). Exploring the mineral-water interface: reduction and reaction kinetics of single hematite (α-Fe_2O_3) nanoparticles. *Chemical Science*, *7*, 1408–1414.
Tang, C. C., MacLean, E. J., Roberts, M. A., Clarke, D. T., Pantos, E., & Prag, A. J. N. W. (2001). The study of Attic black gloss sherds using synchrotron Xray diffraction. *Journal of Archaeological Science*, *28*, 1015–1024.
Thorn, J. (2009). The invention of 'Tarentine' red-figure. *Antiquity*, *183*, 174–183.
Thorn, J., & Glascock, M. (2010). New evidence for Apulian red-figure production centres. *Archaeometry*, *52*, 777–795.
Tite, M. S., Bimson, M., & Freestone, I. C. (1982). An examination of the high gloss surfaces finishes on Greek Attic and Roman Samian wares. *Archaeometry*, *24*, 117–126.
Trendall, A. D. (1967). *The red-figured vases of Lucania; Campania and Sicily*. Oxford University Press.
Trendall, A. D. (1989). *Handbook of red figure vases of south Italy and Sicily*. Thames-Hudson.
Trendall, A. D., & Cambitoglou, A. (1978). *The red-figured vases of Apulia; early and middle Apulian I*. Clarendon.
Trendall, A. D., & Cambitoglou, A. (1982). *The red-figured vases of Apulia; Late Apulian II* (Vol. 1982). Clarendon.
Walton, M., Trentelman, K., Cummings, M., Poretti, G., Maish, J., & Saunders, D. (2013). Material Evidence for Multiple Firings of Ancient Athenian Red-Figure Pottery. *Journal of the American Ceramic Society*, *96*, 2031–2035.
Wan, H., Lv, M., Liu, X., Chen, G., Zhang, N., Cao, Y., Wang, H., Ma, R., & Qiu, G. (2019). Activating Hematite Nanoplates via Partial Reduction for Electrocatalytic Oxygen Reduction Reaction. *ACS Sustainable Chemical Engineering*, *7*, 11841–11849.
Zhao, Q., Yan, Z., Chen, C., & Chen, J. (2017). Spinels: Controlled preparation, oxygen reduction/evolution reaction application, and beyond. *Chemical Reviews*, *117*, 10121–10211.
Zhu, H., Zhang, S., Huang, Y. X., Wu, L., & Sun, S. (2013). Monodisperse $M_xFe_{3-x}O_4$ (M= Fe, Cu, Co, Mn) Nanoparticles and their electrocatalysis for oxygen reduction reaction. *Nano Letters*, *13*, 2947–2951.

SUPPORTING INFORMATION

Additional supporting information may be found in the online version of the article at the publisher's website.

How to cite this article: Doménech-Carbó, A., Giannuzzi, M., Mangone, A., & Giannossa, L. C. (2022). Electrochemical methods to discriminate technology and provenance of Apulian red-figured pottery. I. VIMP and SECM. *Archaeometry*, *64*(6), 1325–1339. https://doi.org/10.1111/arcm.12785